Research Article / *Araştırma Makalesi*

Ege Journal of Medicine / *Ege Tıp Dergisi* 2026; 65 (1): 55-67

Experimental profiling and in silico validation of autophagy and apoptosis-related genes in murine lung cancer and fibroblast cells

Murin akciğer kanseri ve fibroblast hücrelerinde otofaji ve apoptoz genlerinin deneysel profilleme ve in silico validasyonu

Berrin Ozdil[1,2] Yasemin Adalı[3,4] Yasemin Berberoglu[4] Irmak Tutak[4]
Aylin Koseler[4] Huseyin Aktug[5]

[1]Department of Biophysics, Faculty of Medicine, Ege University, Izmir /Türkiye

[2]Department of Physics, Biophysics Laboratory, Izmir Institute of Technology, Izmir/Türkiye

[3]Centre for Public Health, Queen's University Belfast, School of Medicine, Dentistry and Biomedical Sciences, Belfast/United Kingdom

[4] Pamukkale University Medical Faculty, Department of Biophysics, Denizli/Türkiye

[5] Department of Histology and Embryology, Faculty of Medicine, Ege University, Izmir/Türkiye

ABSTRACT

Aim: Autophagy and apoptosis are key programmed cell death pathways that play a critical role in cellular homeostasis. Dysregulation of these pathways is frequently associated with cancer development and progression. Comparing the molecular signatures of tumor and normal cells may provide novel insights into the survival mechanisms adopted by cancer cells.

Objective: The objective of this study was to compare the expression profiles of key autophagy- and apoptosis-related genes between murine lung carcinoma cells and non-malignant fibroblasts and to assess their regulatory interactions using in silico analyses.

Materials and Methods: KLN-205 murine lung carcinoma cells and mouse skin fibroblasts (MSF) were cultured under standard conditions. The mRNA expression levels of *Atg7*, *SQSTM1*, *Beclin-1*, *Caspase-3*, *Caspase-8*, *Caspase-9*, *Bax*, and *Bcl-2* were quantified by RT-qPCR. Normalized data were analyzed using $2^{-\Delta\Delta CT}$ method, and statistical differences between groups were evaluated using unpaired t-tests. In silico analyses were performed to explore broader expression patterns and molecular interactions, including principal component analysis (PCA) and the construction of protein–protein interaction (PPI) networks using the STRING database.

Results: A significant downregulation of *Atg7* was observed in KLN-205 cells compared to MSF ($p < 0.05$). PCA demonstrated distinct clustering of the two cell types, while volcano plots and heatmaps supported the presence of transcriptional differences. STRING network analysis revealed compact interactions between autophagy and apoptosis regulators, with *Beclin-1* and *Caspase-3* as key network hubs. Enrichment analyses identified overrepresented pathways such as 'Autophagy,' 'Apoptosis,' 'p53 signaling,' and 'Mitophagy.'

Conclusion: Our findings indicate that murine lung carcinoma cells exhibit coordinated transcriptional changes in autophagy and apoptosis pathways. In particular, the significant downregulation of Atg7 and altered expression of other key genes suggest a functional suppression of the autophagic machinery and a reprogramming of cell death regulation.

Keywords: Lung cancer, autophagy, apoptosis, KLN-205, gene expression, RT-qPCR, biophysics

Corresponding author: Huseyin Aktug
Department of Histology and Embryology, Faculty of Medicine, Ege University Izmir/Türkiye
E-mail: *huseyin.aktug@ege.edu.tr*
Application date: 14.08.2025 Accepted: 28.10.2025

ÖZ

Amaç: *Otofaji ve apoptoz, hücresel homeostazın korunmasında kritik bir rol oynayan kritik programlanmış hücre ölüm yollarıdır. Bu süreçlerin düzensizliği genellikle kanser gelişimi ve ilerlemesinde rol oynar. Amacımız, murin akciğer karsinomu hücreleri ile malign olmayan fibroblastlar arasındaki anahtar otofaji ve apoptozla ilişkili genlerin ekspresyon profillerini karşılaştırmak ve in silico analizler kullanarak düzenleyici etkileşimlerini değerlendirmektir.*

Gereç ve Yöntem: *KLN-205 murin akciğer karsinomu hücreleri ve fare derisi fibroblastları (MSF) standart koşullar altında kültüre edilmiştir. Atg7, SQSTM1, Beclin-1, Kaspaz-3, Kaspaz-8, Kaspaz-9, Bax ve Bcl-2'nin mRNA ekspresyon seviyeleri RT-qPCR ile ölçülmüştür. Normalize edilen veriler $2^{-\Delta\Delta CT}$ dönüşümü kullanılarak analiz edilmiş ve gruplar arasındaki istatistiksel farklılıklar eşleşmemiş t-testleri ile değerlendirilmiştir. Temel bileşen analizi (PCA) ve STRING veri tabanı kullanılarak protein-protein etkileşimi (PPI) ağlarının oluşturulması dahil olmak üzere daha geniş ekspresyon modellerini ve moleküler etkileşimleri keşfetmek için in silico analizler yapılmıştır.*

Bulgular: *MSF'ye kıyasla KLN-205 hücrelerinde Atg7'de anlamlı bir aşağı regülasyon gözlenmiştir ($p < 0.05$). PCA, iki hücre tipinin farklı kümelenmesini gösterirken, volkan grafikleri ve ısı haritaları transkripsiyonel farkın varlığını desteklemiştir. STRING ağ analizi, otofaji ve apoptoz düzenleyicileri arasında, Beclin-1 ve Kaspaz-3'ün ana ağ merkezleri olarak kompakt etkileşimleri ortaya çıkarmıştır. Zenginleştirme analizleri, 'Otofaji', 'Apoptoz', 'p53 sinyali' ve 'Mitofaji' gibi aşırı temsil edilen yolakları belirlenmiştir.*

Sonuç: *Çalışmamız, murin akciğer karsinomu hücrelerinde otofaji ve apoptoz yolaklarının koordineli transkripsiyonel modülasyonunu vurgulamaktadır. Atg7'nin belirgin aşağı regülasyonu ve diğer anahtar genlerin değişmiş ekspresyonu, otofajik mekanizmanın fonksiyonel olarak baskılanmasını ve hücre ölümü regülasyonunun yeniden şekillenmesini önermektedir.*

Anahtar Sözcükler: *Akciğer kanseri, otofaji, apoptoz, KLN-205, gen ekspresyonu, RT-qPCR, biyofizik*

INTRODUCTION

Autophagy and apoptosis are two evolutionarily conserved mechanisms of programmed cell death that play fundamental roles in tissue homeostasis, stress responses, and cellular quality control (1). Autophagy primarily facilitates the degradation and recycling of damaged organelles and proteins via lysosomal pathways, thereby promoting cell survival under metabolic or oxidative stress. In contrast, apoptosis is a tightly regulated cascade leading to controlled cellular dismantling without eliciting inflammation, essential for development and immune regulation (2). While these processes are distinct, they often intersect and influence one another at multiple molecular checkpoints.

The dysregulation of autophagy and apoptosis is a hallmark of cancer, contributing to tumor initiation, progression, immune evasion, and resistance to therapy. In early stages of tumorigenesis, autophagy may act as a tumor suppressor by eliminating damaged organelles and limiting genomic instability (3). In established tumors, however, autophagy may be adapted to support cell survival under conditions of hypoxia or nutrient deprivation. Similarly, defects in apoptotic signaling, such as overexpression of anti-apoptotic proteins (e.g., *Bcl-2*) or suppression of pro-apoptotic factors (e.g., *Bax, Caspases*), allow cancer cells to evade cell death and continue proliferating despite external insults, including chemotherapy (4).

Given the dual role and therapeutic relevance of these pathways (5), delineating their gene expression patterns in cancerous versus non-cancerous cells can provide valuable mechanistic insights. While several studies have investigated autophagy and apoptosis individually or both in various cancer models (6,7), a combined and comparative expression analysis focusing on both processes in lung cancer and somatic cells remains limited. A previous study by our group investigated autophagy- and mTOR-related gene expression patterns across murine embryonic stem cells, lung cancer cells (KLN-205), and fibroblasts, focusing on developmental context and using a broader panel of genes, along with protein-level assessments (8). The current study builds upon this background by specifically comparing KLN-205 and MSF cells, with a targeted emphasis on the interplay between autophagy and apoptosis pathways. Importantly, this work introduces a distinct set of genes, such

as Atg7 and caspases, applies statistical validation, and incorporates multivariate and network-level in silico analyses, offering new insights into transcriptional regulation in a cancer-specific context. Thus, while thematically related, this study addresses a different biological question with complementary methodology and scope.

In this study, we aimed to investigate the expression profiles of key genes involved in autophagy (*Atg7, SQSTM1, Beclin-1*) and apoptosis (*Caspase-3, Caspase-8, Caspase-9, Bax, Bcl-2*) in murine lung cancer cells (KLN-205) and normal fibroblast (MSF) cells. We utilized quantitative RT-qPCR to assess transcriptional differences and complemented these findings within silico analyses, including PCA, STRING-based protein-protein interaction mapping, and pathway enrichment analysis. By integrating molecular profiling with bioinformatic validation, we aimed to characterize the regulatory mechanisms underlying cell death pathways in a murine lung cancer model and to identify potential targets for future mechanistic or therapeutic investigation. The comparison between KLN-205 and MSF was designed to contrast a malignant phenotype with a non-transformed cell type. Fibroblasts serve as a widely accepted model for baseline gene expression and are frequently used as controls in cancer biology due to their genomic stability and absence of tumor-specific mutations. By using MSF as a reference, we aimed to identify cancer-associated alterations in the expression of autophagy and apoptosis genes that may not simply reflect tissue-specific variability, but rather underlying malignant transformation. This approach enables the characterization of transcriptional signatures that distinguish tumor cells from normal counterparts, offering potential insights into mechanisms of cell death resistance in cancer.

MATERIALS and METHODS

Cell Culture and RNA Extraction

KLN-205 (ATCC) murine lung carcinoma cells and mouse skin fibroblast (MSFs; Clone III8C, ATCC-CRL-2017) cells were cultured under standard conditions using EMEM (Biowest), 10% FBS and McCOys's 5A (Bio Ind) 10% FBS, respectively (8).

Reverse Transcription and Quantitative Real-Time PCR (RT-qPCR)

For total RNA isolation, the cell pellet was lysed using 1 mL of One Step RNA Reagent, then incubated with chloroform and centrifuged (15,000 rpm, 15 min). The supernatant containing total RNA was collected, precipitated with isopropanol, washed with 70% ethanol, and dried. The pellet was dissolved in 20 µL of RNase-DNase-free water, and the total RNA purity and concentration was measured using a NanoDrop.

Complementary DNA (cDNA) was synthesized using a reverse transcription kit containing oligo-dT primers. Following the manufacturer's protocol, 1.5 µg total RNA was used for cDNA synthesis with the OneScript Plus cDNA Synthesis Kit (abm). The mixtures prepared for cDNA synthesis were brought to a final volume of 20 µl with RNase-DNase-free water. The samples were incubated at 55^{o}C for 15 minutes in a Peqlab Primus 25 Thermal Cycler, followed by incubation at 85^{o}C for 5 minutes to stop the reaction. The synthesized cDNA was stored at -20^{o}C until RT-qPCR analysis.

RT-qPCR was performed on a Qiagen Rotor-Gene Q instrument using BlasTaq 2X qPCR MasterMix (abm). Each sample was analyzed in triplicate, with *β-actin* as the reference gene. The primers are shown in Table-1 (OriGene). Data were analyzed via the GeneGlobe Data Analysis platform (Qiagen) using the $2^{-\Delta\Delta CT}$ method.

Table-1. Primer sequences used in gene expression analysis.

Gene	Primer Sequences	NCBI Reference Sequence
B-actin	F: CATTGCTGACAGGATGCAGAAGG R: TGCTGGAAGGTGGACAGTGAGG	NM_007393
Atg7	F: CCTGTGAGCTTGGATCAAAGGC R: GAGCAAGGAGACCAGAACAGTG	NM_028835
SQSTM1	F: GCTCTTCGGAAGTCAGCAAACC R: GCAGTTTCCCGACTCCATCTGT	NM_011018
Beclin-1	F: CAGCCTCTGAAACTGGACACGA R: CTCTCCTGAGTTAGCCTCTTCC	NM_019584

Caspase-3	F: GGAGTCTGACTGGAAAGCCGAA R: CTTCTGGCAAGCCATCTCCTCA	NM_009810
Caspase-8	F: ATGGCTACGGTGAAGAACTGCG R: TAGTTCACGCCAGTCAGGATGC	NM_009812
Caspase-9	F: GCTGTGTCAAGTTTGCCTACCC R: CCAGAATGCCATCCAAGGTCTC	NM_015733
Bax	F: AGGATGCGTCCACCAAGAAGCT R: TCCGTGTCCACGTCAGCAATCA	NM_007527
Bcl-2	F: CCTGTGGATGACTGAGTACCTG R: AGCCAGGAGAAATCAAACAGAGG	NM_009741

Statistical Analysis and Data Transformation

CT values obtained from RT-qPCR were processed in R (version 4.4.1). For each sample, ΔCT values were calculated by subtracting the CT of the reference gene (*ß-actin*) from the CT of the target gene. Normalized expression values were computed as $2^{-\Delta\Delta CT}$, which provides a linear representation of relative transcript abundance. These values were used for downstream statistical comparisons and visualization.

Between-group comparisons (KLN-205 vs. MSF) were conducted using unpaired two-tailed t-tests assuming unequal variances. p-values <0.05 were considered statistically significant. Log_2 fold change values were calculated as:log_2(fold change)=log_2(meanKLN−205meanMSF)\log_2(fold change) =\log_2\left(\frac{\text{mean}_{KLN-205}}{\text{mean}_{MSF}}\right)log2 (fold change)=log2(meanMSFmeanKLN−205)

Data Visualization in R

All visualizations were created in R using the following packages: *ggplot2, ggfortify, pheatmap*, and *factoextra*.

Barplot of log_2 Fold Change

Barplots were generated to visualize the direction and magnitude of gene regulation in KLN-205 cells relative to MSF controls. log_2 fold change values were calculated for each gene and displayed with color-coded bars (blue for upregulated, light blue for downregulated). This representation allows intuitive comparison across genes.

Volcano Plot

A volcano plot was constructed to simultaneously display both fold change and statistical significance for each gene. log_2(fold change) was plotted on the x-axis and -log_{10}(p-value) on the y-axis. Genes meeting both criteria ($|log_2FC| > 0.25$ and $p < 0.05$) were highlighted. This approach helps to distinguish biologically and statistically relevant changes.

Heatmap of Gene Expression

To illustrate overall expression patterns, a heatmap was generated based on log_2(fold change) values using the *pheatmap* package. Genes were clustered by similarity in expression changes, and color gradients (blue to red) represented the direction and strength of regulation.

Principal Component Analysis (PCA) and Biplot

PCA was conducted on $2^{-\Delta\Delta CT}$ normalized values using the prcomp() function in R. The analysis was scaled to account for differences in variance among genes. PCA biplots were visualized using *factoextra::fviz_pca_biplot(),* which displays both the sample distribution (scores) and gene contributions (loadings) in the same plane. Dim1 (PC1) and Dim2 (PC2) accounted for 60% and 22.8% of total variance, respectively. Biological replicates clustered distinctly by group, indicating transcriptomic divergence. Loadings (gene vectors) provided insights into which genes most influenced group separation.

In Silico Analyses

To complement the experimental gene expression data and place the observed transcriptional alterations within broader biological contexts, several in silico analyses were conducted using publicly available databases and bioinformatics tools. The genes evaluated in this study (*Atg7*, *SQSTM1*, *Beclin-1*, *Caspase-3*, *Caspase-8*, *Caspase-9*, *Bax*, and *Bcl-2*) were analysed for their protein-protein interactions, pathway associations, and transcriptional regulatory mechanisms.

Protein-Protein Interaction (PPI) Network Analysis: The STRING v11.5 database (https://string-db.org) was used to generate a protein-protein interaction network. All target genes were entered using their official gene symbols, and interaction scores were filtered with a confidence cut-off of 0.7 (high confidence). Both direct (physical) and indirect (functional) associations were included. Network metrics and clustering patterns were evaluated to identify hub nodes and functional modules.

Pathway Enrichment Analysis: Pathway enrichment analysis was performed using Enrichr (https://maayanlab.cloud/Enrichr) and g:Profiler (https://biit.cs.ut.ee/gprofiler/), focusing on Reactome and KEGG databases. The aim was to determine which biological pathways were overrepresented among the input gene set. Terms with adjusted p-values (FDR) below 0.05 were considered significantly enriched. Pathways related to autophagy regulation, apoptosis signaling, p53 signaling, and mitophagy were of particular interest. We performed functional enrichment analyses using Enrichr and g:Profiler, querying both KEGG and Reactome databases based on the eight target genes (*Atg7*, *SQSTM1*, *Beclin-1*, *Caspase-3*, *Caspase-8*, *Caspase-9*, *Bax*, *Bcl-2*). We considered pathways significantly enriched if the adjusted p-values (FDR) were < 0.05. Enriched pathways were ranked by $\log_{10}$ (FDR) and visualized using barplot representations for comparative interpretation.

RESULTS

To elucidate molecular differences in autophagy- and apoptosis-related gene expression between KLN-205 lung cancer cells and MSF fibroblasts, we conducted a comparative RT-qPCR analysis of eight target genes. Expression values were normalized to *ß-actin* using the $2^{-\Delta\Delta CT}$ method, and fold change was calculated between KLN-205 and MSF groups based on mean values of biological replicates. Statistical significance was evaluated using unpaired two-tailed t-tests.

Fold change analysis reveals gene-specific deregulation in KLN-205 cells

Barplot visualization of $\log_2$ fold change values (Figure-1) illustrated gene-specific trends in expression regulation. *Atg7*, a key initiator of autophagosome formation, exhibited the most notable downregulation in KLN-205 cells ($\log_2$FC ≈ -0.31), consistent with decreased autophagic flux often observed in aggressive tumor contexts. Additionally, *Caspase-8* (-0.20), *Caspase-9* (-0.43), and *Bcl-2* (-0.23) showed decreased expression in KLN-205 compared to MSF, suggesting potential disruption in apoptosis signaling.

Remarkably, a pro-apoptotic Bcl-2 family member *Bax,* was slightly upregulated ($\log_2$FC ≈ +0.14) in KLN-205 cells. This may reflect a stress-related compensatory mechanism or selective pathway activation. The expression of *SQSTM1* and *Beclin-1*, two essential autophagy modulators, remained relatively stable between groups, suggesting that not all autophagic processes are uniformly affected.

Volcano plot highlights Atg7 as a statistically significant target

To simultaneously assess both biological effect size and statistical significance, we generated a volcano plot based on $\log_2$ FC and $-\log_{10}$ (p-value) metrics (Figure-2). Among the genes analyzed, only *Atg7* passed the dual threshold of $|\log_2 FC| > 0.25$ and $p<0.05$, indicating that its downregulation in KLN-205 cells is statistically supported ($p=0.021$).

Although *Caspase-8* and *Caspase-9* approached the fold change cut-off, their p-values remained above 0.05, likely due to sample variability. Notably, *Bax* displayed a positive fold change but had the highest p-value ($p=0.93$), indicating that its change is not statistically meaningful.

Heatmap reveals consistent expression shifts across biological replicates

To better illustrate the determined expression patterns, we visualized $\log_2$FC values as a heatmap (Figure-3), allowing clustering of genes based on expression shifts. Genes such as *Atg7*, *Caspase-9*, and *Bcl-2* clustered together in the heatmap, each showing reduced expression in KLN-205 cells compared to MSF. *Bax* appeared as the only gene consistently more expressed in KLN-205 than in MSF, although the magnitude remained normal.

The consistent downregulation observed across replicates indicates that these expression changes are not due to random variation, but rather reflect biological differences between the two cell types.

PCA reveals distinct clustering of cancerous and non-cancerous samples

To evaluate the overall divergence in transcriptional profiles between KLN-205 and MSF groups, we performed a PCA using $2^{-\Delta\Delta CT}$ normalized data (Figure-4). The first two principal components (PC1 and PC2, denoted as Dim1 and Dim2) accounted for 60% and 22.8% of the total variance, respectively.

Biological replicates clustered tightly within their respective groups, with KLN-205 and MSF samples clearly separating along PC1. This indicates that the overall gene expression signature was sufficiently distinct to differentiate cell types, even in the relatively small gene panel used.

Gene loadings projected as vectors in the PCA biplot revealed that *Atg7*, *Bcl-2*, and *Caspase-8* had the greatest influence on PC1, aligning with the direction of MSF samples and away from KLN-205. This supports the hypothesis that the downregulation of these genes is a major contributor to the transcriptional identity of the cancerous phenotype.

In Silico Results

STRING Network Highlights Connectivity Among Autophagy and Apoptosis Regulators

STRING-based protein–protein interaction analysis demonstrated that the eight genes investigated form a highly interconnected regulatory network (Figure-5). The strongest predicted interactions involved *Caspase-3* with *Caspase-8* (score=0.997) and *Bcl-2* with *Bax* (score=0.998), both canonical players in the intrinsic apoptotic cascade. Interestingly, *SQSTM1* and *Atg7* exhibited a direct link (score=0.898), consistent with their coordinated role in autophagosome formation and cargo recognition (selection of transmembrane proteins).

Notably, *Beclin-1* acted as a functional bridge between the autophagy module to the apoptosis cluster, even though it was not directly in the table due to naming convention differences. These results indicate that in KLN-205 cells, autophagy and apoptosis-related genes are not only transcriptionally altered but also functionally interconnected.

Pathway Enrichment Analysis Highlighting Autophagy and Apoptosis Pathways

Enrichment analysis revealed strong overrepresentation of autophagy-related and apoptosis-related pathways among the gene set (Figure-6). The barplot summarizing pathway enrichment (Figure-6) confirmed that our gene set is significantly involved in key biological processes associated with programmed cell death. The strongest enrichment was observed for the Apoptosis pathway, followed by autophagy-animal, mitophagy, and p53 signaling. These findings reflect the dual functionality of genes like *Atg7*, *Bax*, and *Bcl-2* across both autophagic and apoptotic signaling cascades. The enrichment of p53-related signaling also supports potential transcriptional regulation via canonical tumor suppressor pathways, linking observed gene expression shifts to broader oncogenic processes.

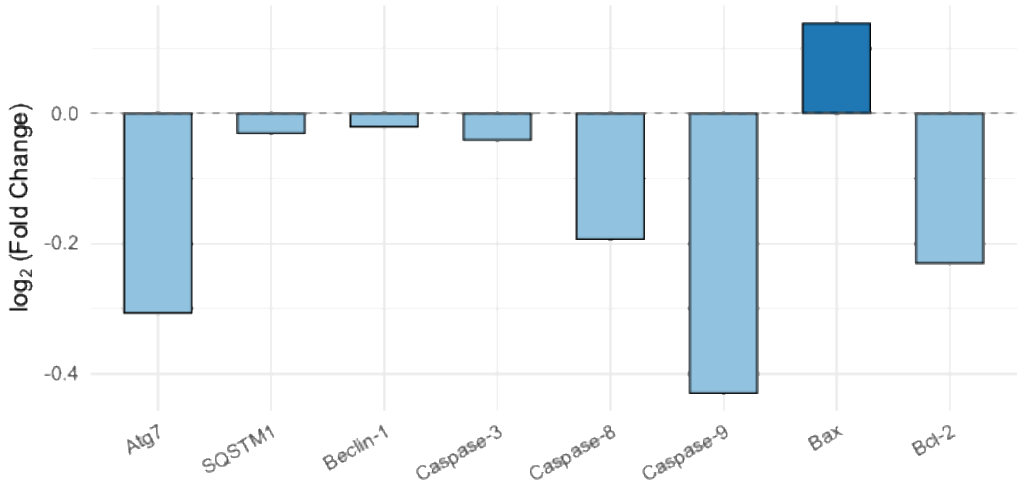

Figure-1. Bar plot of differential gene expression (log_2 fold change) between KLN-205 and MSF cells. The bar plot shows the log_2(fold change) in the expression levels of autophagy and apoptosis related genes in KLN-205 lung cancer cells relative to MSF. Expression values were calculated using the $2^{-\Delta\Delta CT}$ method and normalized to *ß-actin* as a reference gene. Fold changes were then derived by comparing KLN-205 and MSF mean expression values and transformed to log_2 scale. Negative values indicate downregulation in KLN-205 cells, whereas positive values denote upregulation. Notably, *Atg7* displayed the most prominent downregulation (log_2FC=-0.31), suggesting suppression of autophagy initiation mechanisms. *Bax*, associated with pro-apoptotic signaling, was modestly upregulated in KLN-205, while other apoptotic markers such as *Caspase-3*, *Caspase-8*, and *Caspase-9* were slightly downregulated. This barplot provides a comparative overview of gene regulation trends and highlights potential molecular alterations associated with the tumorigenic phenotype.

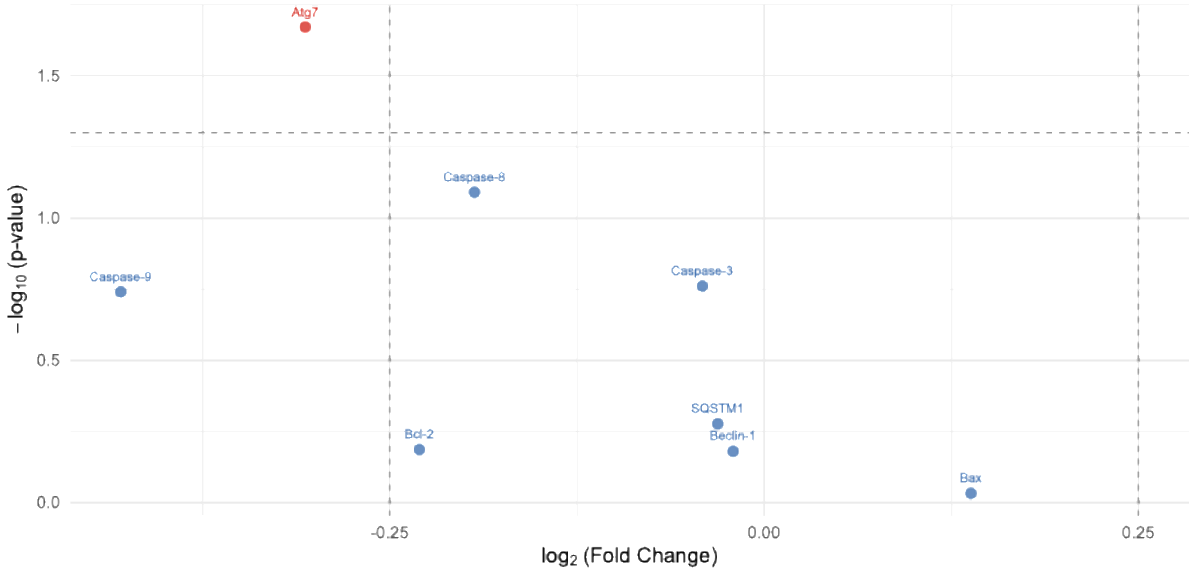

Figure-2. Volcano plot of gene expression differences between KLN-205 and MSF cells. The volcano plot represents differential expression of autophagy- and apoptosis-associated genes between KLN-205 and MSF cells. The x-axis shows log_2 fold change (KLN vs. MSF), while the y-axis represents the statistical significance expressed as $-log_{10}$(p-value). The thresholds for biological and statistical significance were set at $|log_2FC| > 0.25$ and $p < 0.05$, respectively, marked by vertical and horizontal dashed lines. Among all genes tested, only *Atg7* passed both thresholds ($log_2FC=-0.31$, $p=0.021$), indicating significant downregulation in the cancerous cell line. Although genes such as *Caspase-8* and *Caspase-9* showed biologically relevant decreases, they did not meet the strict significance criterion. This plot visually distinguishes genes with potential regulatory importance in lung cancer pathology and underscores *Atg7* as a candidate gene of interest.

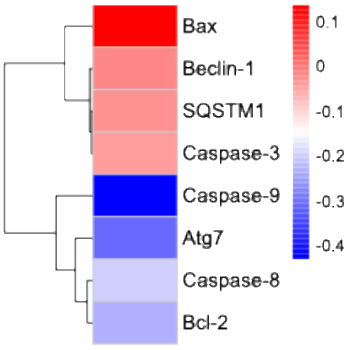

Figure-3. Heatmap of $\log_2$ fold change in gene expression between KLN-205 and MSF cells. The heatmap illustrates the $\log_2$ fold change in expression of key autophagy and apoptosis-related genes in KLN-205 lung cancer cells compared to MSF fibroblasts. Each row represents a gene, and the color intensity reflects the direction and magnitude of regulation (blue = downregulation, red = upregulation). The data are scaled per row to highlight relative differences. *Atg7*, *Caspase-8*, *Caspase-9*, and *Bcl-2* were among the most downregulated genes in KLN-205 cells, while *Bax* displayed upregulation. This heatmap enables a comparative visualization of expression shifts and underlines the observation that autophagy-related pathways, particularly *Atg7*, are suppressed in lung cancer cells.

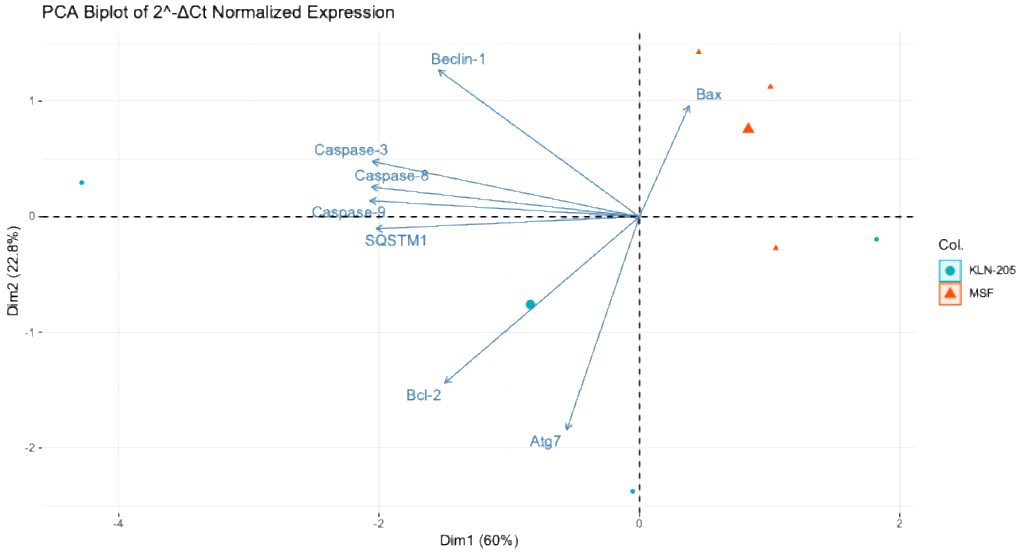

Figure-4. PCA biplot representing $2^{-\Delta CT}$ normalized expression profiles of autophagy- and apoptosis-related genes in KLN-205 lung cancer cells and MSF fibroblasts. Normalized gene expression values were obtained by subtracting *ß-actin* CT values from target gene CT values (ΔCT), followed by transformation to $2^{-\Delta CT}$. PCA was performed using scaled data, and the first two principal components (Dim1 and Dim2) are shown, explaining 60% and 22.8% of the total variance, respectively.

Coloured symbols represent individual biological replicates from each group (KLN-205: cyan circles; MSF: orange triangles). Genes are visualized as loading vectors (arrows), indicating their contribution to the separation of sample groups. Genes pointing in similar directions are positively correlated, while those in opposing directions show inverse relationships. For instance, *Atg7*, *Bcl-2*, and *Bax* show strong contributions along Dim1, suggesting that variations in their expression levels primarily drive the group separation between KLN-205 and MSF. The clustering of KLN-205 replicates separately from MSF reflects fundamental differences in gene expression patterns associated with cell death and survival pathways.

The principal component analysis effectively can be used to discriminate between the two cell types based on the combined transcriptional activity of genes involved in autophagy and apoptosis.

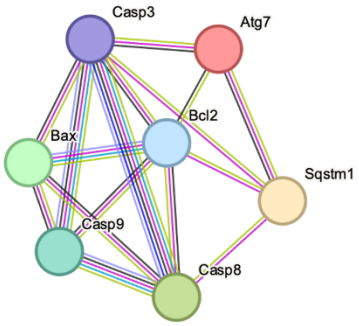

Figure-5. STRING protein–protein interaction (PPI) network of autophagy- and apoptosis-related genes. The network was constructed using STRING v11.5 with a high-confidence interaction score threshold (≥ 0.7) for *Mus musculus*. Pathways with higher bars represent lower FDR values, for instance, stronger statistical support for enrichment and correlation. Three major clusters are visible: an autophagy core module (*Atg7*, *Beclin-1*, *SQSTM1*), an apoptosis execution module (*Caspase-3*, *Caspase-8*, *Caspase-9*, *Bax*, *Bcl-2*), and bridging interactions between these pathways. The strongest interactions included *Caspase-3* ↔ *Caspase-8* (score = 0.997), *Bcl-2* ↔ *Bax* (score = 0.998), and *SQSTM1* ↔ *Atg7* (score = 0.898). This network illustrates the functional connectivity between autophagy initiation and apoptotic signaling in the cell death machinery.

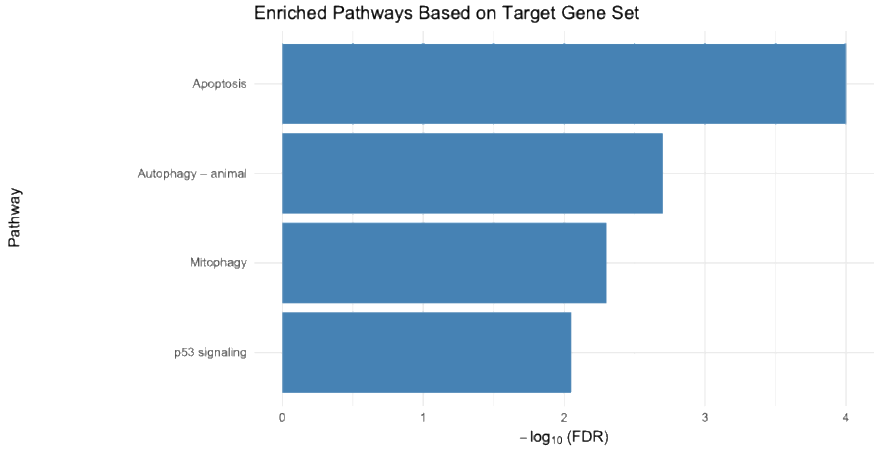

Figure-6. Pathway enrichment analysis of the autophagy- and apoptosis-related genes included in this study. The barplot displays the -$\log_{10}$ transformed adjusted p-values (FDR) for the top enriched pathways obtained from KEGG and Reactome databases using Enrichr. The most significantly enriched pathways were apoptosis, autophagy, mitophagy, and p53 signaling, indicating that the selected gene panel is functionally involved in multiple forms of regulated cell death and stress adaptation. Pathways with higher bars represent lower FDR values, i.e., stronger statistical support for enrichment.

DISCUSSION

This study provides a comparative analysis of autophagy and apoptosis-related gene expression in murine lung carcinoma (KLN-205) and non-cancerous fibroblast (MSF) cell lines, highlighting subtle but biologically meaningful transcriptional shifts. By integrating RT-qPCR with multiple visualization and enrichment approaches, we aimed to uncover potential disruptions in cell death–associated pathways that characterize the tumor phenotype. Our results reveal that KLN-205 cells exhibit a transcriptional signature characterized by significant downregulation of *Atg7*, coupled with moderate alterations in pro- and anti-apoptotic genes such as *Caspase-8, Caspase-9, Bcl-2,* and *Bax*. These findings suggest a shift in cell death regulation associated with the malignant phenotype.

Among the evaluated genes, *Atg7* was identified as the most significantly downregulated gene in

KLN-205 cells, with both fold change and p-value consistently confirming its suppression. *Atg7* is a critical initiator of autophagosome formation and is often deregulated in cancers where autophagy is reprogrammed to support survival under cellular stress (9,10). Its suppression in KLN-205 cells may reflect a strategic silencing of canonical autophagic pathways, possibly favoring alternative survival strategies or immune evasion. Previous study showed similar downregulation in *Atg7, Atg10* and *Beclin-1* in acute B-lymphoblastic leukemia patient (11). Besides, our findings align with those of Oltulu et al. (8), who profiled autophagy- and mTOR-related gene expression in KLN-205, mouse skin fibroblasts, and mouse embryonic stem cells. Their results also indicated a reduced expression of key autophagy genes, including *Atg10*, in KLN-205 cells relative to fibroblasts. This observation is consistent with our findings and further supports the idea that of autophagy may be a common characteristic of lung carcinoma cells. Notably, while their study utilized a broader pathway approach including mTOR and incorporated protein-level detection via immunofluorescence, our results provide complementary transcriptional evidence, thereby and reinforcing the reliability of the in silico validation.

The expression patterns of apoptosis-related genes were more complex and less uniform. While *Caspase-3, Caspase-8, and Caspase-9* showed mild downregulated in KLN-205 cells, these changes did not reach statistical significance. The anti-apoptotic gene *Bcl-2* and the pro-apoptotic gene Bax showed opposite trends, with *Bax* displayed slight upregulation. This opposing expression pattern is consistent with the idea that cancer cells may retain a partially functional apoptotic machinery while at the same time strengthening their anti-apoptotic defences. However, since these changes were not statistically significant, apoptosis evasion in KLN-205 cells may instead involve post-transcriptional or post-translational regulatory mechanisms. *Caspase-3* has been proposed to be a key regulator for chemoresistance in breast cancer (12). Moreover, in cancer biology, functional mutations or alternative splicing events in caspase genes have been widely reported, resulting in altered protein activity (13,14). While our study did not directly assess mutational status, the differences between gene expression patterns and canonical apoptotic behaviour in KLN-205 cells suggests that there may be underlying genetic or epigenetic alterations that warrant further investigation. Notably, *Caspase-3* has been associated with chemoresistance in several tumour types, including breast cancer, highlighting its potential role as both a biomarker and therapeutic target (15–17).

PCA further supported transcriptional divergence between KLN-205 and MSF cells. Despite the relatively limited gene panel, PCA achieved a clear group separation, with *Atg7, Caspase-8,* and *Bcl-2* contributing strongly to variance. In cancer transcriptomics, PCA has been effectively used to classify tumor versus normal tissues and to define molecular subtypes from functional gene sets (18). This suggests that even a focused set of cell death–related genes can robustly distinguish malignant from non-malignant profiles.

STRING-based protein–protein interaction (PPI) analysis provided additional functional context, revealing dense interconnectivity between autophagy and apoptosis regulators. Notably, *Beclin-1* emerged as a central node linking both pathways, supporting previous evidence that autophagy and apoptosis form a highly integrated cell death mechanism (19). Enrichment analyses of Reactome and KEGG pathways confirmed significant associations with canonical signaling cascades such as autophagy, apoptosis, mitophagy, and p53 signaling, all of which are implicated in tumour biology and therapeutic resistance. While this study offers valuable insight into transcriptional modulation of cell death mechanisms, it is not without limitations. The findings are based solely on mRNA levels; further validation at the protein and functional levels (e.g., autophagic flux assays, caspase activity measurements) would strengthen the mechanistic interpretation.

In conclusion, our findings suggest that KLN-205 lung cancer cells exhibit synchronized repression of autophagy and partial reprogramming of apoptosis-related genes, highlighting *Atg7* as a potential therapeutic target for modulating autophagy in tumor settings. These transcriptional signatures, supported by interaction and enrichment analyses, offer mechanistic insight into the altered regulation of cell death pathways in cancer and may serve as a basis for future studies exploring therapeutic targeting of these systems.

Our findings align with those of Oltulu et al. (8), who profiled autophagy and mTOR-related gene expression across mouse embryonic stem cells (mESCs), KLN-205 lung cancer cells, and mouse skin fibroblasts (MSFs). In contrast, their study adopted broader perspective on pathway regulation, including mTOR signalling, and combined RT-qPCR with immunofluorescence techniques. Within this framework, they observed reduced expression of several autophagy-related genes (e.g., Atg10) in KLN-205 cells compared to MSF. This observation is consistent with our data showing *Atg7* downregulation in KLN-205 cells, further supporting the notion that autophagy may be transcriptionally suppressed in these tumour cells. The concordance between these two studies reinforces the relevance of cell-type-specific autophagy gene modulation in lung carcinoma and underscores the utility of combining experimental gene profiling with in silico analysis to explore mechanistic overlaps in cancer biology. Among the target genes evaluated, *Atg7* emerged as the most significantly downregulated gene in KLN-205 cells, with both fold change and p-value supporting its suppression. *Atg7* is a key initiator of autophagosome formation and is often found deregulated in cancers where autophagy is reprogrammed to promote survival under stress. Its suppression here may reflect a strategic silencing of the canonical autophagic machinery, possibly favouring alternative survival routes or contributing to immune evasion.

Apoptosis-related genes displayed more complex patterns. While *Caspase-3*, *Caspase-8*, and *Caspase-9* were mildly downregulated in KLN-205 cells, the anti-apoptotic gene *Bcl-2* and pro-apoptotic *Bax* showed opposite trends, with *Bax* modestly upregulated. This conflicting expression pattern is consistent with the idea that cancer cells maintain a delicate balance between survival and death signaling, often retaining the machinery for apoptosis while simultaneously upregulating anti-apoptotic controls. However, none of these changes reached statistical significance, suggesting that post-transcriptional or post-translational modifications may also play a role in regulating apoptosis in this model.

The PCA biplot clearly separated KLN-205 and MSF replicates, supporting the idea that even a limited gene panel can reveal meaningful transcriptional differences when appropriately normalized and analyzed. Importantly, genes such as *Atg7*, *Caspase-8*, and *Bcl-2* contributed strongly to this separation, further validating their role in defining the cellular phenotype.

PPI analysis added functional interpretation to our findings, revealing strong interconnections between autophagy and apoptosis regulators. The identification of *Beclin-1* as a central hub linking both modules supports previous reports that autophagy and apoptosis are closely integrated processes forming cell death network (20). Moreover, pathway enrichment analyses confirmed that the selected genes are significantly involved in canonical pathways such as ‘Autophagy,’ ‘Apoptosis,’ and ‘p53 signalling’ all of which are relevant to tumour progression and therapeutic resistance.

While this study provides a focused snapshot of transcriptional regulation in two distinct cell types, it also has limitations. The analysis was restricted to mRNA levels, and protein-level validation of key genes would strengthen the conclusions.

In conclusion, our findings suggest that KLN-205 lung cancer cells exhibit coordinated transcriptional attenuation of autophagy and apoptosis-associated genes, particularly *Atg7*, which may function as a key rate-limiting factor in the regulation of cell death. The observed expression profile, supported by pathway enrichment and interaction analyses, offers key regulatory shifts with malignant transformation and defines potential molecular vulnerabilities that could be exploited for therapeutic intervention.

CONCLUSION

This study reveals transcriptional alterations in autophagy and apoptosis-related genes between KLN-205 lung cancer cells and non-malignant fibroblasts, with *Atg7* standing out as a significantly downregulated gene in the tumour. Integrating RT-qPCR validation with multivariate statistical analyses and in silico enrichment approaches strengthens the interpretation that these gene-level shifts are not isolated but reflect broader disruptions in cell death regulation. Pathway enrichment and network analyses demonstrate a functional crosstalk between autophagy and apoptosis, highlighting their joint role in supporting tumor cell survival.

Taken together, these findings suggest that the suppression of canonical autophagic machinery, accompanied by a subtle reprogramming of apoptotic signaling, may present a molecular strategy by which KLN-205 cells sustain viability

and evade stress-induced death. Further validation at the protein and functional levels is needed; however, *Atg7* and its associated regulators appear to be promising targets for future mechanistic investigations or therapeutic interventions in lung cancer models.

Conflicts of interest: Authors declared no conflict of interest.

References

1. Qian S, Long Y, Tan G, Li X, Xiang B, Tao Y, vd. Programmed cell death: molecular mechanisms, biological functions, diseases, and therapeutic targets. MedComm [Internet]. 01 Aralık 2024;5(12):e70024. Available at: https://doi.org/10.1002/mco2.70024
2. Gómez-Virgilio L, Silva-Lucero M-D-C, Flores-Morelos D-S, Gallardo-Nieto J, Lopez-Toledo G, Abarca-Fernandez A-M, vd. Autophagy: A Key Regulator of Homeostasis and Disease: An Overview of Molecular Mechanisms and Modulators. Cells. Temmuz 2022;11(15).
3. Jalali P, Shahmoradi A, Samii A, Mazloomnejad R, Hatamnejad MR, Saeed A, vd. The role of autophagy in cancer: from molecular mechanism to therapeutic window. Front Immunol [Internet]. 2025;Volume 16. Available at: https://www.frontiersin.org/journals/immunology/articles/10.3389/fimmu.2025.1528230
4. Saddam M, Paul SK, Habib MA, Fahim MA, Mimi A, Islam S, vd. Emerging biomarkers and potential therapeutics of the BCL-2 protein family: the apoptotic and anti-apoptotic context. Egypt J Med Hum Genet [Internet]. 2024;25(1):12. Available at: https://doi.org/10.1186/s43042-024-00485-7
5. Yun CW, Jeon J, Go G, Lee JH, Lee SH. The Dual Role of Autophagy in Cancer Development and a Therapeutic Strategy for Cancer by Targeting Autophagy. Int J Mol Sci. Aralık 2020;22(1).
6. Tutak I, Ozdil B, Uysal A. Voxtalisib and low intensity pulsed ultrasound combinatorial effect on glioblastoma multiforme cancer stem cells via PI3K/AKT/mTOR. Pathol Pract. 2022;239:154145.
7. Dikici O, Ozdil B, Yesin TK, Dikici A, Adalı Y, Aktug H. Time-Dependent Effects of Low-Intensity Pulsed Ultrasound on Apoptosis and Autophagy in Malignant Melanoma Stem Cells. J Cell Mol Med. Haziran 2025;29(12):e70687.
8. Oltulu F, Kocaturk DC, Adali Y, Ozdil B, Acikgoz E, Gurel C, vd. Autophagy and mTOR pathways in mouse embryonic stem cell, lung cancer and somatic fibroblast cell lines. J Cell Biochem. Ekim 2019;120(10):18066–76.
9. Xu Y, Qian C, Wang Q, Song L, He Z, Liu W, vd. Deacetylation of ATG7 drives the induction of macroautophagy and LC3-associated microautophagy. Autophagy [Internet]. 03 Mayıs 2024;20(5):1134–46. Available at: https://doi.org/10.1080/15548627.2023.2287932
10. Ostacolo K, López García de Lomana A, Larat C, Hjaltalin V, Holm KY, Hlynsdóttir SS, vd. ATG7(2) Interacts With Metabolic Proteins and Regulates Central Energy Metabolism. Traffic [Internet]. 01 Nisan 2024;25(4):e12933. Available at: https://doi.org/10.1111/tra.12933
11. Hasanpour SZ, Allah Bakhshian M, Mohammadi MH, Ghasemian SO, Gholami-Ahangaran M. Beclin1, Atg10 and Atg7 genes expressions as autophagy mediators in acute B-lymphoblastic leukemia. Hum Gene [Internet]. 2024;41:201311. Available at: https://www.sciencedirect.com/science/article/pii/S277304412400055X
12. Devarajan E, Sahin AA, Chen JS, Krishnamurthy RR, Aggarwal N, Brun A-M, vd. Down-regulation of caspase 3 in breast cancer: a possible mechanism for chemoresistance. Oncogene. Aralık 2002;21(57):8843–51.
13. Ghavami S, Hashemi M, Ande SR, Yeganeh B, Xiao W, Eshraghi M, vd. Apoptosis and cancer: mutations within caspase genes. J Med Genet [Internet]. 01 Ağustos 2009;46(8):497 LP – 510. Available at: http://jmg.bmj.com/content/46/8/497.abstract
14. Park JY, Park JM, Jang JS, Choi JE, Kim KM, Cha SI, vd. Caspase 9 promoter polymorphisms and risk of primary lung cancer . Hum Mol Genet [Internet]. 15 Haziran 2006;15(12):1963–71. Available at: https://doi.org/10.1093/hmg/ddl119

15. Qaed E, Liu W, Almoiliqy M, Mohamed R, Tang Z. Unleashing the potential of Genistein and its derivatives as effective therapeutic agents for breast cancer treatment. Naunyn Schmiedebergs Arch Pharmacol [Internet]. 2025;398(4):3321–43. Available at: https://doi.org/10.1007/s00210-024-03579-6
16. Pu X, Storr SJ, Zhang Y, Rakha EA, Green AR, Ellis IO, vd. Caspase-3 and caspase-8 expression in breast cancer: caspase-3 is associated with survival. Apoptosis [Internet]. 2017;22(3):357–68. Available at: https://doi.org/10.1007/s10495-016-1323-5
17. Boice A, Bouchier-Hayes L. Targeting apoptotic caspases in cancer. Biochim Biophys Acta - Mol Cell Res [Internet]. 2020;1867(6):118688. Available at: https://www.sciencedirect.com/science/article/pii/S016748892030046X
18. Baranovsky A, Ivanov T, Granovskaya M, Papatsenko D, Pervouchine DD. Transcriptome analysis reveals high tumor heterogeneity with respect to re-activation of stemness and proliferation programs. PLoS One. 2022;17(5):e0268626.
19. Kang R, Zeh HJ, Lotze MT, Tang D. The Beclin 1 network regulates autophagy and apoptosis. Cell Death Differ. 2011;18(4):571–80.
20. Marquez RT, Xu L. Bcl-2:Beclin 1 complex: multiple, mechanisms regulating autophagy/apoptosis toggle switch. Am J Cancer Res [Internet]. 2012/02/15. 2012;2(2):214–21. Available at: https://pubmed.ncbi.nlm.nih.gov/22485198